Impact Compressive Failure of GFRP Unidirectional Composites

Jianming Yuan* and Nobuo Takeda
Center for Collaborative Research (CCR), The University of Tokyo
4-6-1 Komaba, Meguro-ku, Tokyo 153-8904, Japan

Anthony M. Waas
Department of Aerospace Engineering, University of Michigan
FXB Bldg., Ann Arbor, MI 48109-2118, USA

ABSTRACT

Compressive impact tests of unidirectional glass fiber reinforced vinyl ester matrix composites (GFRP) were carried out using the split Hopkinson pressure bars. The dynamic stress-strain curves of unidirectional composites of six different fiber volume fractions and pure matrix were obtained at the strain rate of 10^3 s^{-1}. Impact recovery tests were also performed to study the impact compressive damage evolution in composites. The temperature dependence up to 100°C was examined to study the temperature effect on the compressive strength. Quasi-static compressive tests of the same specimens at the strain rate of 10^{-3} s^{-1} were also conducted for comparison. Failed specimens were examined by optical microscopy. Kinking followed by splitting was found to be the main controlling failure mechanism. GFRP exhibited ductile failure for lower fiber volume fractions, but brittle failure for higher fiber volume fractions. As the temperature increased, the failure mode changed from kinking to microbuckling. Experiments showed that the strain rate has a strong effect on the compressive strength. Some theoretical prediction of the compressive strength was also made based on the failure mechanism and test data.

Key Words: GFRP, impact compression, fiber volume fraction, temperature effect.

1. INTRODUCTION

The compressive response of unidirectional composites is an essential part of the basic property data required for the optimized design of composite structures. For the fiber reinforced polymer matrix composite, the compressive strength is usually much lower than the tensile strength. This factor limits the exploitation of these materials. Although numerous studies relating to the compressive behavior have been conducted, the mechanism of composite failure in compression has not been well understood. The main mechanism of unidirectional composite failure in compression was found to be microbuckling, kinking, fiber crush, and matrix failure /1/. Much of this understanding of compressive failure mechanism has been obtained on the basis of static loading. Relatively little work has been conducted to investigate the dynamic compressive behavior of unidirectional composites /2,3/.

Compressive failure of highly aligned composites is catastrophic in nature. It is difficult to observe and

* Present address: Department of Mechanical and Production Engineering, National University of Singapore, 10 Kent Ridge Crescent, Singapore 119260.

record the damage evolution process in a static test. Because the recovery impact test /4/ is capable of loading a specimen to a certain level followed by unloading it for microscopic and related analysis, it can be used in studying the compressive failure process.

In this paper, the dynamic compressive behavior of glass fiber reinforced unidirectional vinyl ester was studied experimentally. Quasi-static compressive tests of these composites were also conducted for comparison. Research focused on the compressive damage evolution and failure mode in these unidirectional composites as well as the factors influencing the compressive strength. The factors included the strain rate, the fiber volume fraction and the temperature. Prediction of the compressive strength was also analyzed based on the experimental results and some analytical models.

2. EXPERIMENTS

2.1. Test specimens

Reinforcement and matrix resin used in this study were E-glass fiber and vinyl ester (Derakane 411-C50), respectively. The unidirectional GFRP composites with six different fiber volume fractions ranging from 10% to 60% were fabricated within a long glass tube, then, circular cylindrical specimens of approximately 7 mm diameter and 5 mm length were machined. Specimens of pure matrix with the same geometry as composites were also fabricated. Specimens of all fiber volume fractions were tested under impact and static loadings. GFRP of $V_f = 40\%$ was used in impact recovery tests in order to study the compressive damage evolution under impact loading. Both $V_f = 50\%$ GFRP and pure matrix were used in impact tests at high temperature up to 100°C in order to study the temperature effect on the compressive failure mechanism. Two to four samples were used in each test.

2.2. Test procedures

Impact compressive tests were performed using the split Hopkinson pressure bars (SHPB), in which the stress waves in the input and output bars were recorded to calculate the dynamic stress-strain curve of specimens. In order to improve the accuracy of the dynamic stress-strain curves obtained from SHPB tests of GFRP whose failure strain is usually small, a method considering wave propagating in specimens was applied in data processing of SHPB tests /5/. Recovery impact compressive tests were performed using an improved compression-type SHPB apparatus shown in Fig. 1

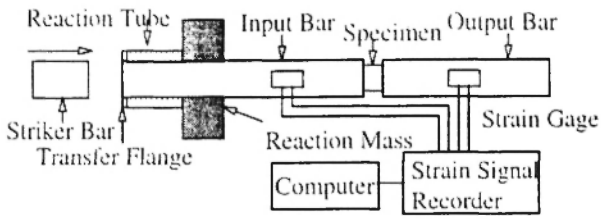

Fig. 1: Improved compression-type SHPB apparatus.

/2,4/. Compared with the ordinary SHPB apparatus, the improved SHPB apparatus added a transfer flange, a reaction tube and a reaction mass. When the striker bar impacted the input bar, the incident and transmitted waves were recorded as shown in Fig. 2. The unloading wave was produced immediately after the loading wave. Hence, once the specimen was loaded in compression only by the initial compressive segment of the stress pulse, the induced damage could be kept intact by an

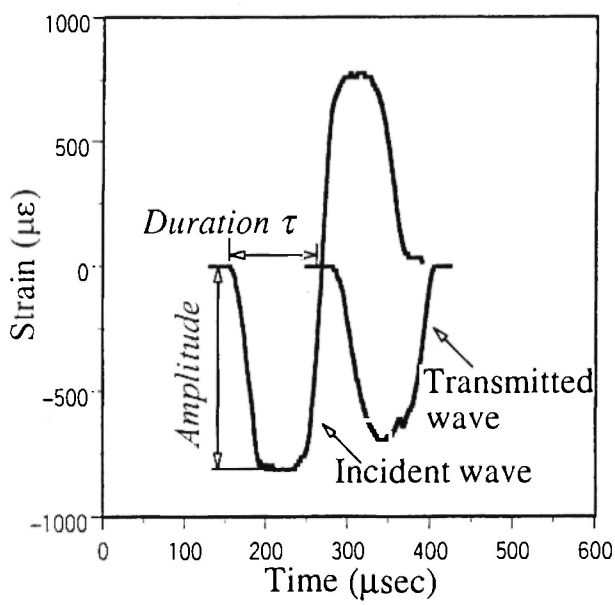

Fig. 2: Recorded waves in impact recovery tests

immediate unloading for later microscopic observation. Adjusting the amplitude and duration of the incident wave resulted in different impact compressive loading levels of the specimen.

Impact tests at high temperature were conducted by using a heat cable to heat specimens to a desired temperature, and the temperature was measured by a thermocouple and controlled properly (Fig. 3). Failed or recovered GFRP specimens were observed by optical microscopy because this GFRP was transparent.

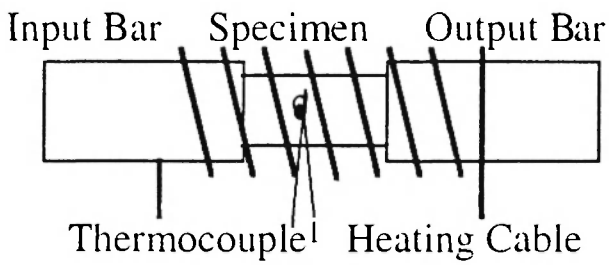

Fig. 3: Impact test at high temperature

Steel rings were used to confine specimen ends in some tests (Fig. 4). The inner diameter of the ring was a little larger than the diameter of the specimen so that their contact was loose. The rings restrained radial expansion of the specimen ends under compressive loading. By comparing the recorded stress-strain curves with and without using rings, it was found that the rings did not alter the mechanical behavior of the specimen. Tests also showed the rings could prevent post-failure in specimens, and therefore, it is helpful in recovering failed specimens for microscopic analysis /6/.

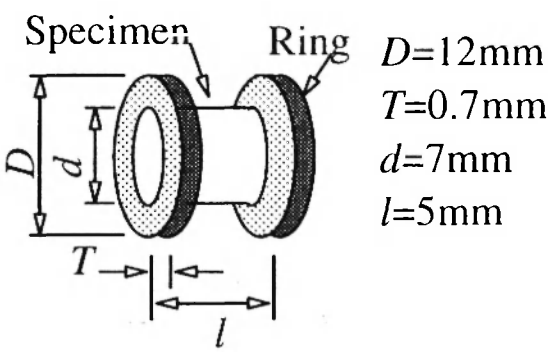

Fig. 4: Specimen and rings

3. TEST RESULTS AND ANALYSIS

3.1. Effect of fiber volume fraction and strain rate

The typical stress-strain curves of GFRP of different fiber volume fractions and matrix under static and impact loadings are shown in Figs. 5 and 6,

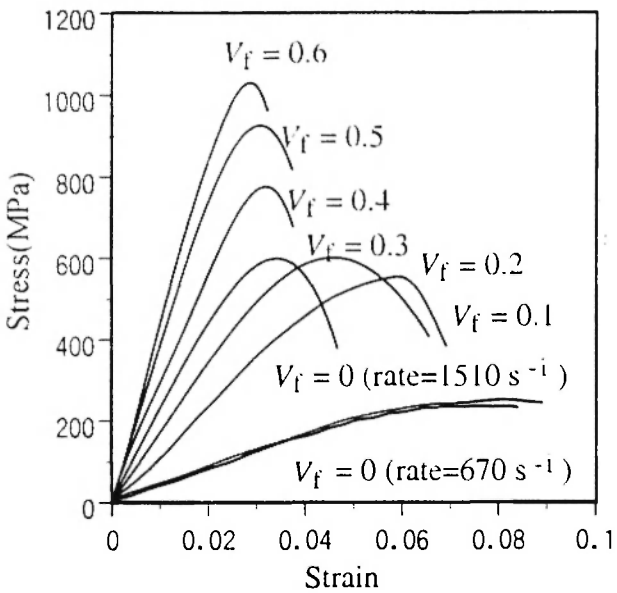

Fig. 5: Stress-strain curves of GFRP and matrix under impact loading (strain rate $\cong 10^3$ s^{-1})

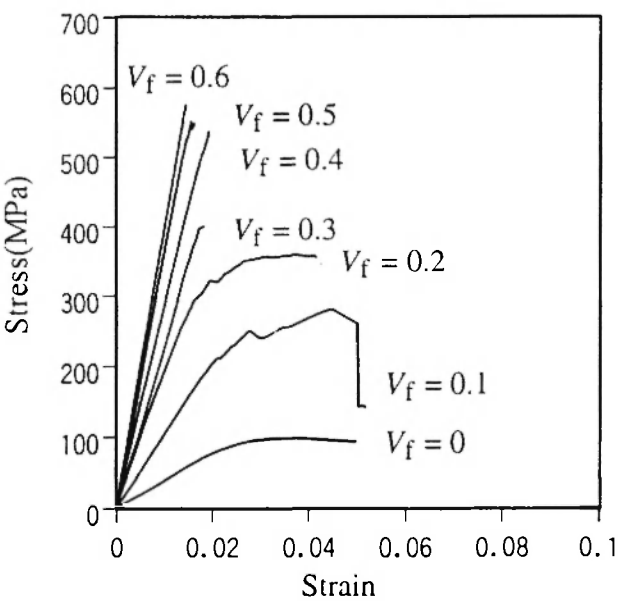

Fig. 6: Stress-strain curves of GFRP and matrix under static loading (strain rate $\cong 10^{-3}$ s^{-1})

respectively. Figure 7 shows the compressive strength of GFRP versus the fiber volume fraction under static and impact loadings.

The failure of GFRP composites changes from ductile to brittle at the fiber volume fraction of 30% - 40% for both static and impact loadings (Figs. 5 and 6). A corresponding nonlinear increase of the compressive strength is noted (Fig. 7). The ratio between the dynamic compressive strength and the static one ranges from 2.5 for pure matrix to 1.7 – 1.8 for GFRP with high fiber volume fractions (Fig. 7).

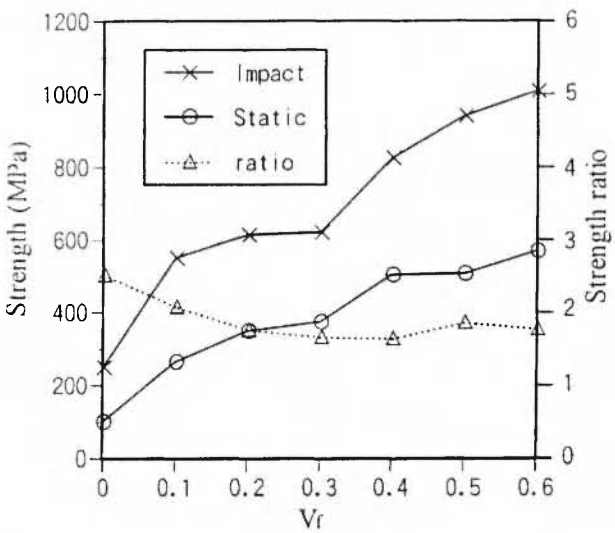

Fig.7: Compressive strength of matrix and GFRP with different fiber volume fractions

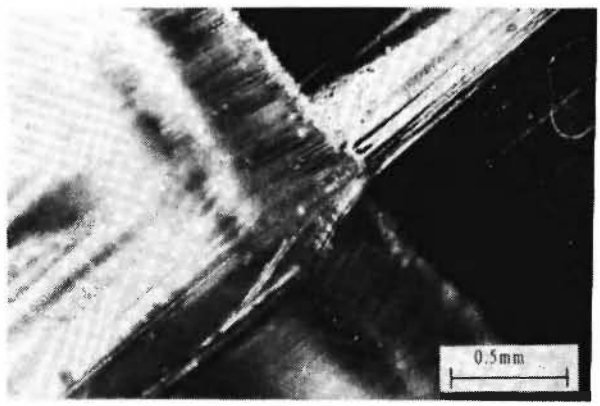

(a) on the surface (V_f = 40%)

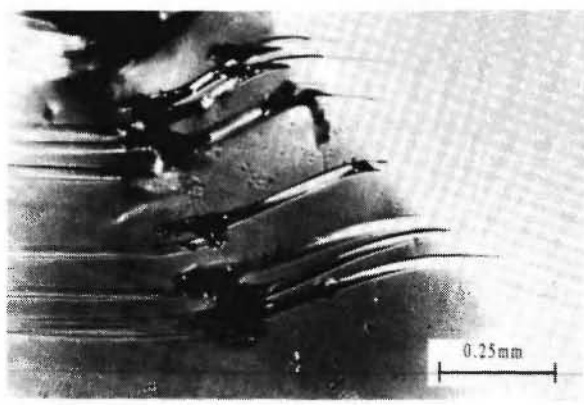

(b) in the interior (V_f = 10%)

Fig. 8: Kinking occurred (a) on the surface (V_f = 40%) and (b) in the interior of GFRP (V_f = 10%).

3.2. Compressive failure mechanism and damage evolution process

Both kinking and longitudinal splitting were found in failed GFRP specimens. Figure 8 shows a kinking band occurring on the surface and in the interior of specimens. When the fiber volume fraction was very small, the interior kinking band could be seen (Fig. 8(b)). For a higher fiber volume fraction, by carefully separating GFRP along the crack of longitudinal splitting, two types of kinking bands in Fig. 9 were found on the separated surface, i.e., the kinking band occurred in plane and out of plane. From Figs. 8 and 9, it can also be found that splitting occurred in the region of the kinking band and some fibers were broken by tensile stresses due to bending.

Impact recovery tests further revealed the compressive damage evolution in GFRP. Figure 10 shows three different damage states under different impact loading levels. Under a low impact loading level, an initial damage (whitening area) occurred first in the region near the specimen ends (Fig. 10(a)). Under a higher impact load, a kinking band was formed (Fig. 10(b)), and then some splitting was also formed (Fig. 10(c)). Experiments showed that no damage in specimens occurred if the loading level was less than 92% of the compressive strength. The loading levels in Figs. 10(a), (b) and (c) are estimated as approximately

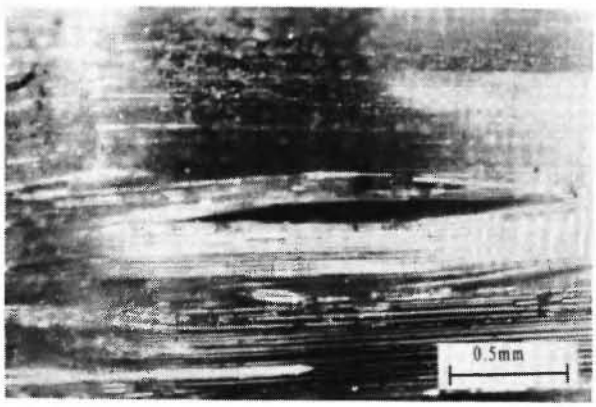

(a) in-plane (V_f = 30%)

(b) out-of-plane (V_f = 20%)

Fig. 9: Kinking bands in the interior of GFRP: (a) in-plane (V_f =30%) and (b) out-of-plane (V_f =20%).

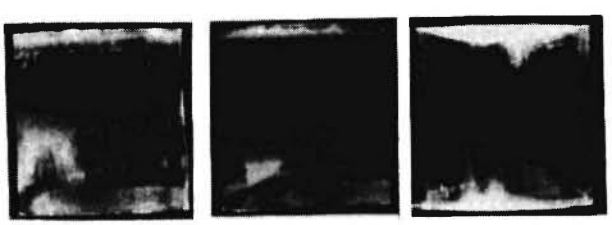

(a) (b) (c)

Fig. 10: Impact compressive damage evolution in GFRP (V_f=40%).

95%, 97% and 99% of the compressive strength, respectively. By observing Figs. 8, 9 and 10, it is concluded that the compressive failure mechanism of GFRP is fiber kinking followed by longitudinal splitting. Figure 11 is a schematic of the failure mechanisms in Figs. 8 and 9. It also shows the global view of the kinking of Figs. 8 and 9 in the specimen. The longitudinal splitting is the result of the required kinetic compatibility of fiber kinking (Fig. 11).

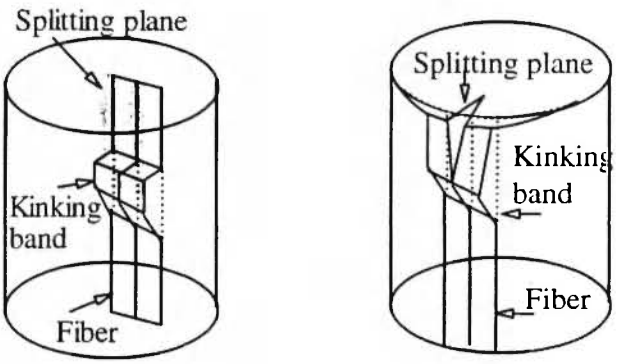

(a) interior kinking (b) surface kinking

Fig. 11: Compressive failure mechanism in GFRP: (a) interior kinking and (b) surface kinking.

Figure 12 shows the stress-time curves of specimens under different loading levels in impact recovery tests. The sample *A* experienced kinking and extensive splitting. Its stress-time curve shows that the specimen load dropped sharply and its duration is much shorter than that of the incident compressive wave. This means that its loading ability was almost totally lost during the loading period. The sample *B* contained kinking and a little splitting. Its stress-time curve shows it had a long duration and a relatively flat top. The final load drop was due to the unloading of the incident loading wave. This means the specimen still had some loading ability. The sample *C* had no damage, and the load drop was due to the unloading of the incident loading wave. The sample *D*, whose two ends were constrained by rings only, had a little splitting, and its stress-time curve is similar to those of samples *B* and *C*. Hence, the splitting is the main factor for the specimen to lose the total loading ability, and specimens only with kinking damage still keep some loading ability.

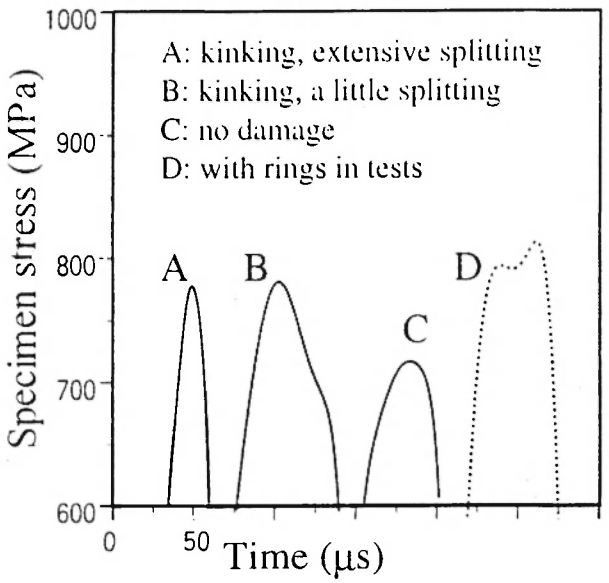

Fig. 12: Stress-time curves in impact recovery tests.

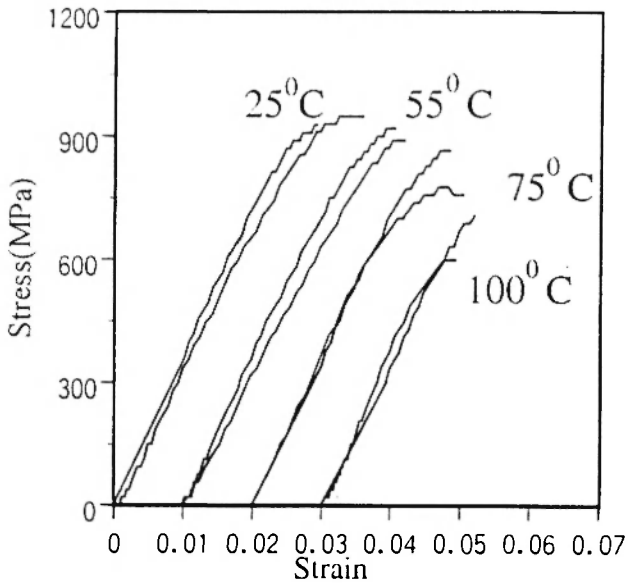

Fig. 14: Dynamic stress-strain curves of GFRP at different temperatures (V_f=50%).

3.3. Temperature effect on the failure mechanism

Figures 13 and 14 show dynamic stress-strain curves at different temperatures of pure matrix and GFRP (V_f= 50%), respectively. Both the modulus and strength of pure matrix are temperature-dependent (Fig. 13), while the modulus of GFRP is not sensitive to temperature but the dynamic compressive strength decreases significantly at approximately 75°C (Fig. 14). Figure 15 shows the temperature effect on some mechanical properties of composites and matrix. At 100°C, it was found that the failure mode changed to fiber buckling (Fig. 16). In the specimen which failed at 100°C, fiber buckling and matrix whitening were found in the whole region of the specimen. However, only fiber kinking could be observed in some locations in the specimen which failed at 25°C.

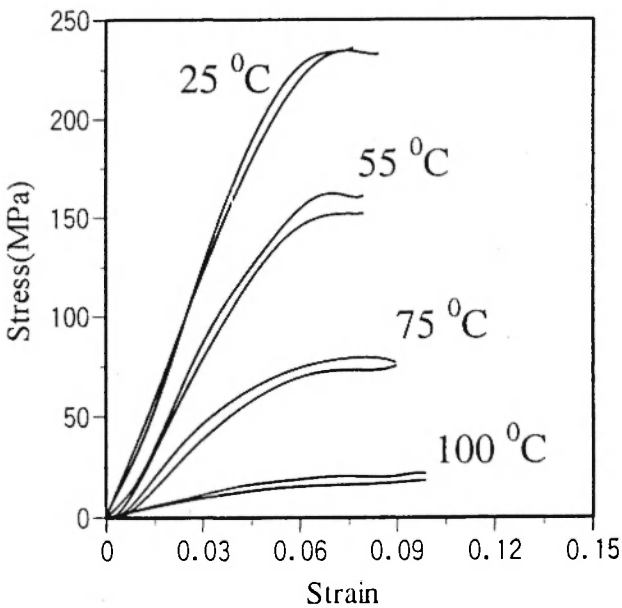

Fig. 13: Dynamic stress-strain curves of matrix at different temperatures.

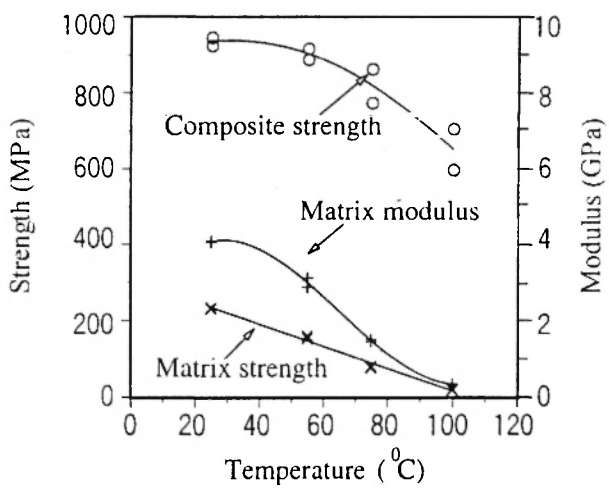

Fig. 15: Comparison of temperature effect on mechanical properties of composite (V_f =50%) and matrix.

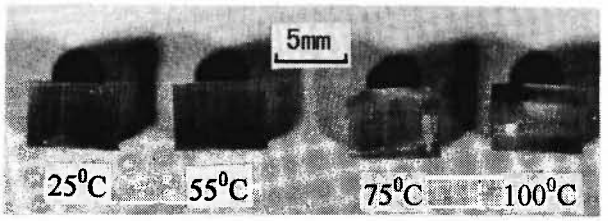

Fig. 16: Failure modes at different temperatures.

4. PREDICTION OF COMPRESSIVE STRENGTH

4.1. Kinking-controlled compressive strength

From the above test results, it is concluded that the same failure mechanism of kinking-splitting controls the dynamic and static compressive failures of the composite with higher fiber volume fractions, but for lower fiber volume fractions, the final controlling factor of compressive strength is the compressive property of the matrix.

It is known that the kinking phenomenon in unidirectional composites is related to the shear property of the composite as well as the initial misalignment of fibers. Misaligned fibers easily undergo microbuckling or kinking under compressive loading. Taking account of matrix plastic deformation and the initial fiber misalignment, Budiansky /7/ provided a predicted compressive strength of unidirectional composites as

$$\sigma_c = \frac{G_{LT}}{1+\phi_0/\gamma_{LT}} \qquad (1)$$

where ϕ_0/γ_{LT} is the ratio of the fiber misalignment angle to the in-plane shear yield strain of the composite, G_{LT} is the composite shear modulus.

The predicted compressive strength based on Eqn. (1) is plotted in Fig. 17 with the following simplification and approximation: $G_{LT} = G_m/(1-V_f)$, $G_m = E_m/2(1+\nu_m)$, Poisson's ratio of matrix $\nu_m = 0.35$, and $E_m = 4.2$ GPa. Here G_m and E_m are the shear modulus and Young's modulus of matrix, respectively. The values of $Y(=\phi_0/\gamma_{LT})$ under impact and static loadings are determined by data fitting.

From Fig. 17, we obtain $\gamma_{LT}^{dynamic}/\gamma_{LT}^{static} = Y^{static}/Y^{dynamic} = 5.0/2.5 = 2.0$. On the other hand, from the test

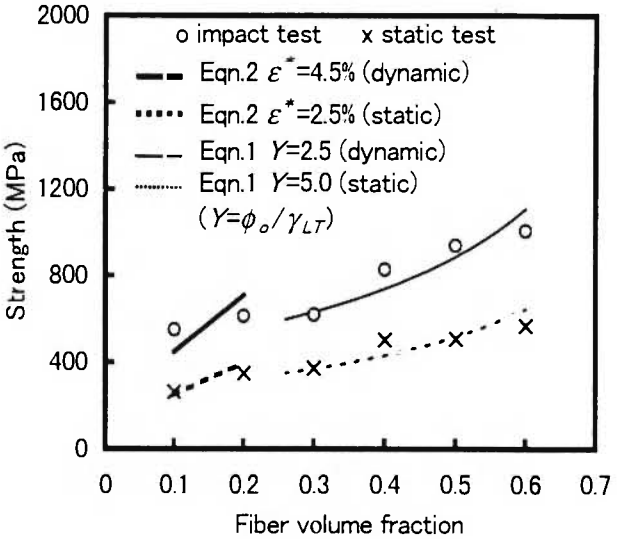

Fig. 17: Comparison of the predicted compressive strength with test data.

results of matrix shown in Figs. 5, 6 and 7, we obtain $\varepsilon_{failure}^{dynamic}/\varepsilon_{failure}^{static} = 8/3.3 \approx 2.4$. and $\sigma_{failure}^{dynamic}/\sigma_{failure}^{static} \approx 2.5$, and $E^{dynamic} \approx E^{static}$. Moreover, it is confirmed by the experiments that the shear strength of the laminate is close to that of the matrix /8/. Hence, the value of $\gamma_{LT}^{dynamic}/\gamma_{LT}^{static}$ is physically reasonable because it is similar to the values of $\varepsilon_{failure}^{dynamic}/\varepsilon_{failure}^{static}$ or $\sigma_{failure}^{dynamic}/\sigma_{failure}^{static}$. Considering the simplification and approximation used in the analysis, it is concluded that Eqn. (1) is qualitatively correct for predicting the compressive strength for the kinking controlled failure.

4.2. Matrix-controlled compressive strength

For composites with lower fiber volume fractions, the stress-strain curves show ductile failures. Supposing the final strength is controlled by the yield of matrix, the rule of mixture results in a compressive strength of unidirectional composite as

$$\sigma_c = \left(E_m V_m + E_f V_f\right)\varepsilon^* \qquad (2)$$

where ε^* is the yield strain of the matrix under compression, which can be determined from the stress-strain curves of matrix in Figs. 5 and 6. The predicted

compressive strength based on Eqn. (2) is also plotted in Fig. 17. From Fig. 17, it can be found that the predicted compressive strength is reasonably consistent with the test data.

4.3. Temperature effects on compressive strength

At high temperatures, the compressive failure mechanism is fiber microbuckling. Only considering matrix elastic deformation, Rosen's model gives the compressive strength as /9/:

$$\sigma_c = \frac{G_m}{1-V_f} \tag{3}$$

Comparison of the predicted compressive strength based on Eqns. (3) and (1) with test data is shown in Fig. 18. Equation (1) underestimates the compressive strength at higher temperature; this is because of the assumption that $Y = \phi_0/\gamma_{LT} = 5$ in the calculation. In reality, the yield shear strain of composite, γ_{LT}, is temperature-dependent, and therefore, Y should also be temperature-dependent. Compared with Equation (1), Equation (3) can predict the compressive strength more close to the test data for $V_f = 50\%$ at 100°C, although there is still some discrepancy between the predicted and measured values.

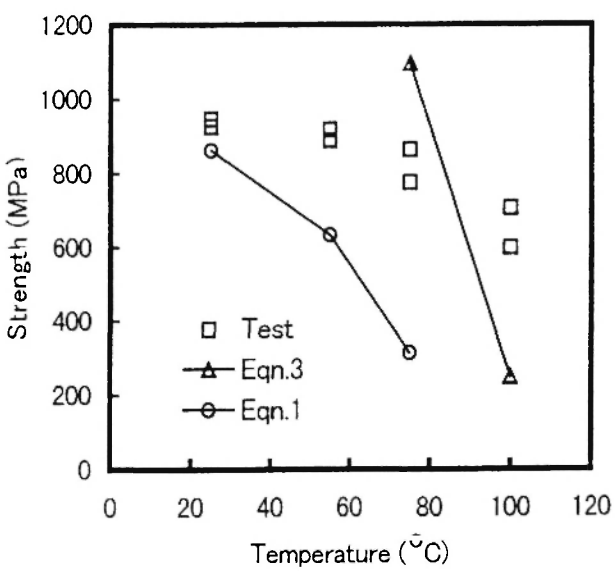

Fig. 18: Comparison of the predicted impact compressive strength with test data at high temperatures ($V_f = 50\%$).

4. CONCLUSIONS

The dynamic and static compressive behavior of GFRP was studied experimentally. The following conclusions were drawn:

1. The compressive failure mechanism is fiber kinking followed by longitudinal splitting. The longitudinal splitting is caused due to the required kinematic compatibility of fiber kinking. Splitting causes specimens to lose the total loading capability, but those with only kinking damage still keep some loading capability. Glass fibers often break under the tensile stresses due to bending in the kinking band. As the fiber volume fraction increases, the compressive failure changes from ductile to brittle, which results in a nonlinear increase in the compressive strength.

2. Within the tested temperature range up to 100°C, the Young's modulus of composites is constant. The compressive failure in GFRP changes from kinking at room temperature to microbuckling at 100°C. The compressive strength decreases significantly at approximately 75°C. The temperature has a strong effect on the mechanical behavior of matrix. The decrease in the compressive strength at high temperatures is due to the temperature-softening effect of matrix.

3. Although the composites have the same compressive failure mechanism under impact and static loadings, the strain rate has a strong effect on the compressive failure strength. Under impact loading, the increase in the compressive strength is due to the increase in the matrix strength.

4. Although both interior and surface kinkings were observed, the interior kinking was found to occur in most cases. The test results showed no difference in the strength for the two kinds of kinking. Regarding the strength prediction, it should be noted that only a qualitative comparison can be made at present, because some parameters used in the prediction were not determined accurately. They were obtained from data fitting and some simplified calculations.

ACKNOWLEDGMENTS

The authors acknowledge the support of the grant-in-aid for international cooperation from Monbusho throughout the present study.

REFERENCES

1. C.R. Schultheisz and A.M. Waas, "Compressive failure of composites, Part 1: Testing and micro-mechanical theories", *Prog. Aerospace Sci.*, **32**, 1-42 (1996).
2. N. Takeda, L. Wan, M. Hiramatsu and J. Yuan, "Characterization of effects of strain rate and temperature on impact compressive damage progress of glass fiber reinforced composite", *Trans. JSME, Ser. A*, **63** (616), 2598-2603 (1993) [in Japanese].
3. J. Lankford, "Shear versus dilatational damage mechanisms in the compressive failure in fiber-reinforced composite", *Composites, Part A*, **28A**, 215-222 (1997).
4. S. Nemat-Nassar, J.B. Isaacs and J.E. Starrett, "Hopkinson techniques for dynamic recovery experiments", *Proc. R. Soc. Lond.*, **A435**, 371-391 (1991).
5. J. Yuan, N. Takeda and A.M. Waas, "A note on the data processing in the split Hopkinson pressure bar tests", *Exp. Techniques*, **22** (5), 31-24 (1998).
6. J. Yuan, N. Takeda. D.Y. Song and A.M. Waas, "Experimental study on dynamic compressive failure of unidirectional CFRP composites", *Mater. Sci. Research Int.*, **5** (3),202-205 (1999).
7. B. Budiansky, "Micromechanics", *Computers and Structures*, **16** (1-4), 3-12 (1983).
8. D. Hull and T.W. Clyne, *An Introduction to Composite Materials* (2nd Ed.), Cambridge University Press, Cambridge, 1996; pp. 177-178.
9. B.W. Rosen, "Mechanics of composite strengthening", *Fiber Composite Materials*, ASM, 1965; pp. 37-75.